Supplementary Material

1. XRD

Diffractograms of ZnO samples calcined at 400°C, 500°C, 600°C, and 700°C are shown in Figure S1. In all analyzed samples, peaks corresponding to ZnO with a hexagonal wurtzite structure (JCPDS 036-1451) were detected [1]. As the calcination temperature increased, the intensity of the ZnO diffraction peaks increased, indicating greater crystallinity of the material [2-4]. This suggests that higher calcination temperatures provide sufficient energy for the crystallites to orient at equilibrium positions [5].

In samples calcined at 400°C and 500°C, in addition to ZnO diffraction peaks, peaks at 2θ angles of 11.2°, 32.8°, 33.5°, 37.8° and 58.1° were detected, corresponding to hexagonal nanosheets of simonkolleite [6]. The calcination temperature influences the amount of simonkolleite in the sample. The simonkolleite content reached 10.4% and 7% at calcination temperatures of 400°C and 500°C, respectively, indicating incomplete decomposition of simonkolleite. Increasing the calcination temperature to 600°C resulted in complete decomposition of simonkolleite, consistent with the results of Moezzi et al. [7]. XRD patterns obtained after sample calcination at 600°C and 700°C reveal that zincite was identified as the only crystalline phase.

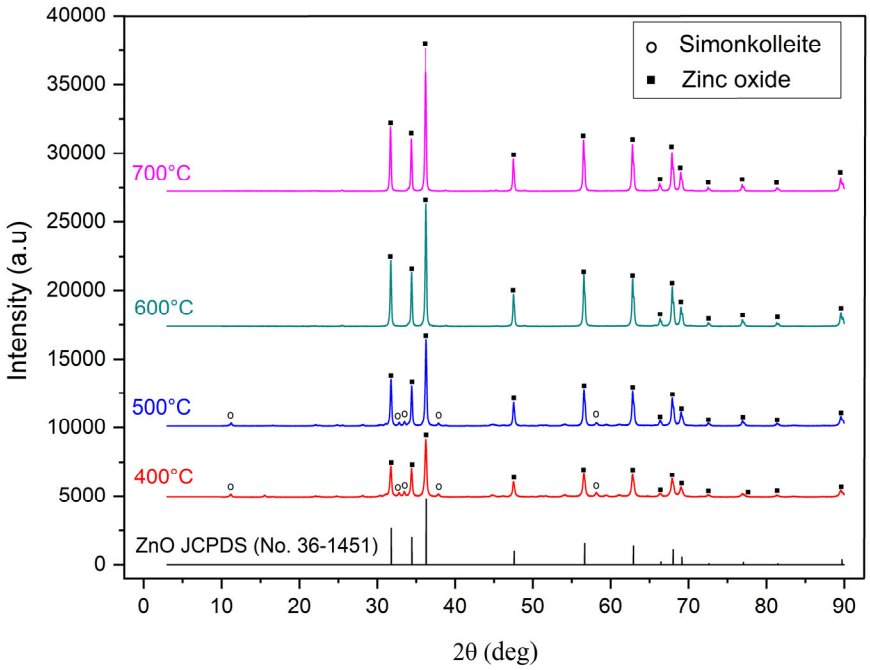


Figure S1. XRD diffractograms of ZnO samples calcined at different temperatures.

As the samples calcined at 400°C and 500°C contained an impurity in addition to ZnO, a detailed analysis of the crystal structure of the samples calcined at 600°C and 700°C was conducted to identify the optimal material for doping with graphene oxide. The structural parameters of ZnO calcined at 600°C and 700°C are shown in Table S1.

Table S1. Structural parameters of ZnO calcined at 600°C and 700°C.

Sample	D (nm)	*a* (Å)	*c* (Å)	*c*/*a*	L (nm)	V (Å^3)	δ (nm^{-2})	ε (%)
JCPDS	/	3,249	5,206	1,602	1,9767	47,622	/	/
600°C	38,2096	3,251	5,206	1,601	1,9782	47,649	$6{,}8494 \cdot 10^{-4}$	0,0897
700°C	38,2538	3,255	5,211	1,601	1,9805	47,812	$6{,}8336 \cdot 10^{-4}$	0,0896

The crystallite size and intensity of the (101) peaks increase as the calcination temperature rises. Additionally, the (101) peak narrows at higher temperatures, indicating improved crystallinity of ZnO. The increase in crystallite size at higher calcination temperatures can be attributed to elevated surface energies, which promote grain growth [2, 3, 8-11].

The crystal lattice parameters of ZnO are in close agreement with the standard values reported in the JCPDS database (Table S1). A slight increase in the lattice constants with increasing calcination temperature was observed, indicating the formation of point defects such as oxygen vacancies and zinc antisite defects [12]. High-temperature calcination increases the kinetic energy of atoms within the ZnO lattice, facilitating the release of oxygen atoms and promoting the formation of oxygen vacancies [3, 13], as confirmed by the decrease in the c/a ratio relative to the standard value [14]. The increase in the lattice parameters *a* and *c* with rising calcination temperature directly results in an expansion of the unit cell volume (Table 1), reflecting a relaxation of the ZnO crystal lattice and the formation of oxygen vacancies. The bond length increases with higher calcination temperature due to thermal expansion (Table 1) [15].

The dislocation density of ZnO decreases as the calcination temperature increases (Table 1). Higher calcination temperatures provide more thermal energy, which facilitates the diffusion of atoms from the crystal interior to the grain boundaries, enabling their redistribution and reducing line defects and dislocation density [16]. Additionally, because dislocation density is inversely proportional to the square of the crystallite size, an increase in crystallite size results in lower dislocation density [17].

Microstrain in ZnO samples depends on the calcination temperature. As calcination temperature increases, crystallite size increases, leading to decreased dislocation density and lattice relaxation, which reduces microstrain [2, 18]. A decrease in dislocation and strain density indicates improved crystallinity of the samples [19].

The results indicate that increasing the calcination temperature from 600°C to 700°C increases the number of oxygen vacancies and the sample's crystallinity. The increase in crystallinity reduces the recombination of photogenerated pairs, allowing more efficient use of charge carriers in photocatalytic processes. At the same time, the presence of oxygen vacancies increases the number of active sites for the adsorption of organic pollutants.

2. FTIR

To identify functional groups and assess the purity of ZnO synthesised from waste Zn-C batteries and calcined at temperatures from 400°C to 700°C, FTIR analysis was performed. The results, shown in Figure S2, indicate that all tested samples exhibit an intense peak in the region from 400 to 600 cm^{-1},

corresponding to stretching and deformation of the Zn–O bond at the surface of the photocatalyst, and a peak at 900 cm^{-1}, representing a weak vibration of the Zn–O bond [20-22]. The presence of these peaks indicates the formation of ZnO nanoparticles [23]. For samples calcined at 400°C and 500°C, in addition to the peaks indicating ZnO, a broad absorption band between 3400 and 3500 cm^{-1} was observed, along with a peak at about 720 cm^{-1}, attributed to stretching vibrations of the O–H bond [24,25]. These absorption peaks are characteristic of simonkolleite [8, 26]. The results indicate that in ZnO samples calcined at 400°C and 500°C, simonkolleite was also identified in addition to ZnO. In contrast, ZnO samples calcined at higher temperatures exhibited only absorption peaks corresponding to ZnO. The FTIR analysis results are consistent with those of the XRD analysis.

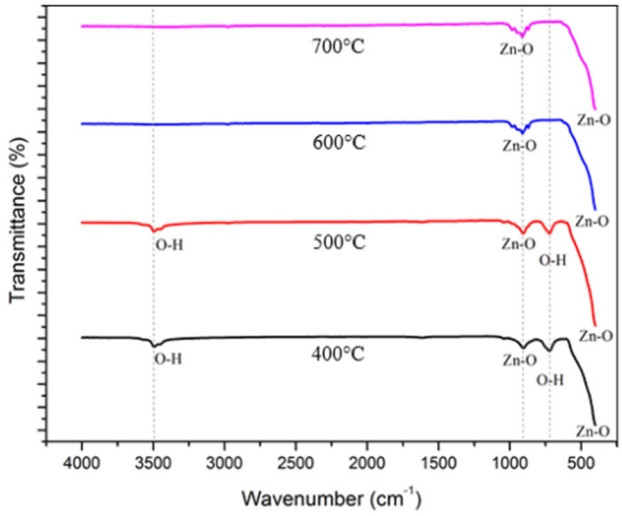


Figure S2. FTIR spectra of ZnO samples calcined at different temperatures.

3. Photocatalytic activity of ZnO NPs

The photocatalytic activity of ZnO nanoparticles calcined at 600°C and 700°C was evaluated based on the efficiency of photocatalytic degradation of malachite green during 90 minutes of exposure to UVA radiation. The results are shown in Figure S3 and indicate that the efficiency of photocatalytic degradation increases with increasing calcination temperature. This trend is also supported by previous research by Nedelkovski et al. [14] and Nguyen and Nguyen [1]. The higher photocatalytic activity of the ZnO sample calcined at 700°C can be attributed to the presence of oxygen vacancies. At higher calcination temperatures, the kinetic energy of atoms in the ZnO lattice increases, facilitating the release of oxygen atoms and the creation of oxygen vacancies [2, 3]. Oxygen vacancies serve as effective sites for dye molecule adsorption and also promote the separation of photogenerated pairs, reducing their recombination and increasing the efficiency of photocatalytic decomposition. As the calcination temperature increases, the crystallinity of ZnO improves, reducing resistance to charge transfer [3]. This enables faster electron transport to the catalyst surface and leads to the formation of more hydroxyl radicals, which act as oxidants in the photocatalytic degradation reactions of malachite green.

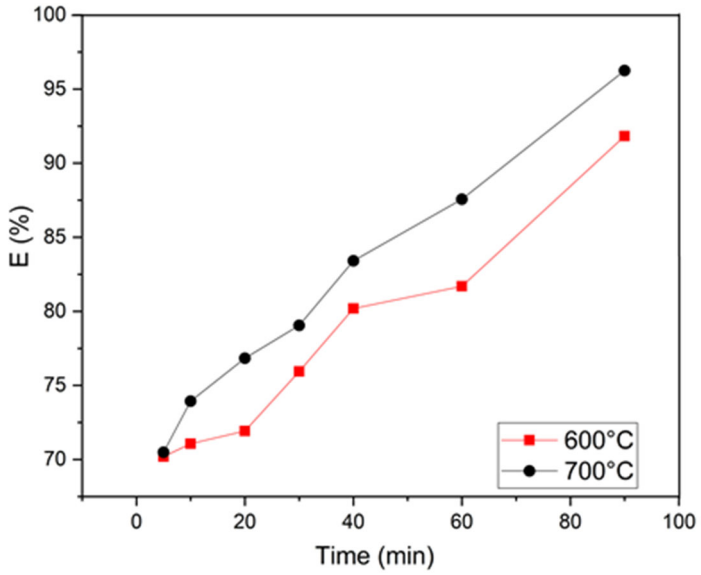


Figure S3. Effect of ZnO calcination temperature on the efficiency of photocatalytic decomposition of malachite green.

The degradation kinetics of malachite green in the presence of ZnO samples were studied using a pseudo-first-order model, which is widely applied to describe photocatalytic processes in heterogeneous systems [14]. The linear relationship of $\ln(C_t/C_0)$ as a function of time clearly confirms that the decomposition of malachite green in the presence of ZnO follows pseudo-first-order kinetics (Figure S4). The rate constant of photocatalytic degradation of MG in the presence of ZnO calcined at 700°C was 0.02271 min^{-1}, while in the presence of ZnO calcined at 600°C it was 0.01455 min^{-1}. This indicates that ZnO calcined at 700 °C has higher photocatalytic activity. Its good crystallinity, phase purity, and high photocatalytic activity make ZnO calcined at 700 °C the most suitable material for GO modification.

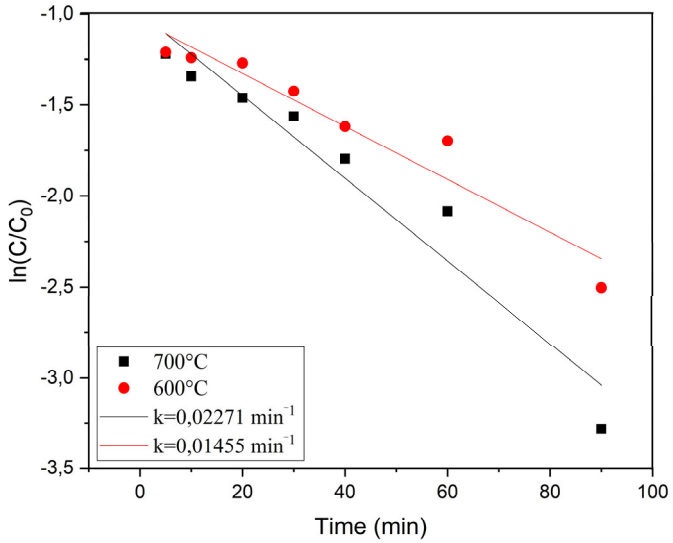


Figure S4. Kinetic analysis of the photocatalytic degradation of MG using ZnO calcined at 600°C and 700°C.

References

1. Nguyen, N.T.; Nguyen, V.A. Synthesis, Characterization, and Photocatalytic Activity of ZnO Nanomaterials Prepared by a Green, Nonchemical Rout. *J. Nanomater.* **2020**, *2020*, 1-8. https://doi.org/10.1155/2020/1768371
2. Parra, M.R.; Haque, F.Z. Aqueous chemical route synthesis and the effect of calcination temperature on the structural and optical properties of ZnO nanoparticles. *J. Mater. Res. Technol.* **2014**, *3*, 363-369. https://doi.org/10.1016/j.jmrt.2014.07.001
3. Golsheikh, A.M.; Kamali, K.Z.; Huang, N.M.; Zak, A.K. Effect of calcination temperature on performance of ZnO nanoparticles for dye-sensitized solar cells. *Powder Technol.* **2018**, *329*, 282–287. https://doi.org/10.1016/j.powtec.2017.11.065
4. Singh, R.P.P.; Hudiara, I.S.; Rana, S.B. Effect of calcination temperature on the structural, optical and magnetic properties of pure and Fe-doped ZnO nanoparticles. *Mater Sci Pol* **2016**, *34*, 451-459. https://doi.org/10.1515/msp-2016-0059
5. Belay, A.; Bekele, B.; Reddy, C.; A.R. Effects of Temperature and Polyvinyl Alcohol Concentrations in the Synthesis of Zinc Oxide Nanoparticles. J Nanotechnol Material Sci 2018, 5, 44-50. https://www.chalcogen.ro/51_BelayA.pdf
6. Li, S.; Chen, X.; Wang, X.; Xiong, Y.; Yan, Y.; Tan, Z.; Yang, X.; Li, Y. Simonkolleite Coating on Poly(Amino Acids) to Improve Osteogenesis and Suppress Osteoclast Formation in Vitro. Polymers 2019, 11, 1505. https://doi.org/10.3390/polym11091505
7. Moezzi, A.; Cortie, M.; McDonagh, A. Transformation of zinc hydroxide chloride monohydrate to crystalline zinc oxide. Dalton Trans. 2016, 45, 7385-7390. https://doi.org/10.1039/C5DT04864H
8. Radovanović, M.B.; Simonović, A.T.; Petrović Mihajlović, M.B.; Tasić, Ž.Z.; Antonijević, M.M. Application of Graphite Electrodes Prepared from Waste Zinc−Carbon Batteries for Electrochemical Detection of Xanthine. Chemosensors 2025, 13, 282. https://doi.org/10.3390/chemosensors13080282
9. Sharma, V.; Sharma, J.K.; Kansay, V.; Sharma, V.D.; Sharma,A.; Kmar, S.; Sharma, A.K.; Bera, M.K. The effect of calcination temperatures on the structural and optical properties of zinc oxide nanoparticles and their influence on the photocatalytic degradation of leather dye. *Chem Phys Impact* **2023**, *6*, 100196. https://doi.org/10.1016/j.chphi.2023.100196
10. Baharudin, K.B.; Abdullah, N., Derawi, D. Effect of calcination temperature on the physicochemical properties of zinc oxide nanoparticles synthesized by coprecipitation. *Mater. Res. Express* **2018**, *5*, 125018. DOI: 10.1088/2053-1591/aae243
11. Kaewsaenee, J.; Singhaset, M.T.; Roongraung, K.; Kemacheevakul, P.; Chuangchote, S. Polymer-Assisted Coprecipitation Synthesized Zinc Oxide Nanoparticles and Their Uses for Green Chemical Synthesis via Photocatalytic Glucose Conversions. *ACS Omega* **2023**, *8*, 43664−43673. https://doi.org/10.1021/acsomega.3c05183
12. Özgür, Ü.; Alivov, Y.I.; Liu,C.; Teke,A.; Reshchikov, M.A.; Doğan, S.; Avrutin, V.; Cho, S.–J.; Morkoç, H. A comprehensive review of ZnO materials and devices. *J. Appl. Phys.* **2005**, *98*, 041301. https://doi.org/10.1063/1.1992666
13. Ni, Z.; Chen, X.; Su, L.; Shen, H.; Yin, C. Effect of Calcination Temperature in Large-Aperture Medium-Entropy Oxide (FeCoCuZnNa)O on CO_2 Hydrogenation for Light Olefins. *Catalysts* **2024**, *14*, 818. https://doi.org/10.3390/catal14110818

14. Nedelkovski, V.; Radovanović, M.; Medić, D.; Stanković, S.; Hulka, I.; Tanikić, D.; Antonijević, M. Enhancing Wastewater Treatment Through Python ANN-Guided Optimization of Photocatalysis with Boron-Doped ZnO Synthesized via Mechanochemical Route. *Processes* **2025**, *13*, 2240. https://doi.org/10.3390/pr13072240
15. Lin, K.–H.; Sun, S.–J.; Ju, S.–P.; Tsai, J.–Y.; Chen, H.–T.; Hsieh, J.–Y. Observation of the amorphous zinc oxide recrystalline process by molecular dynamics simulation. *J. Appl. Phys.* **2013**, *113*, 073512. https://doi.org/10.1063/1.4789956
16. Mostafa, S.; Yeasmin, S.; Pranto, M.H.; Reza, S.M.; Rashid, T.U.; Das, H.; Rahman, M.; Habib, A. Annealing-induced optimization of greensynthesized ZnO nanoparticles for improved nanopriming in sustainable agriculture. *Nanoscale Adv.* **2025**, *7*, 5589. https://doi.org/10.1039/D5NA00354G
17. Zhao, M.–J.; Sun, Z.–T.; Zhang, Z.–X.; Geng, X.–P.; Wu, W.–Y.; Lien, S.–Y.; Zhu, W.–Z. Suppression of Oxygen Vacancy Defects in sALD–ZnO Films Annealed in Different Conditions. *Materials* **2020**, *13*, 3910. https://doi.org/10.3390/ma13183910
18. Saidani, A.; Boudraa, R.; Fendi, K.; Benouadah, L.; Benabbas, A.; Djermoune, A.; Salvestrini, S.; Bollinger, J.–C.; Alayyaf, A.A.; Mouni, L. Effect of Calcination Temperature on the Photocatalytic Activity of Precipitated ZnO Nanoparticles for the Degradation of Rhodamine B Under Different Light Sources. *Water* **2025**, *17*, 32. https://doi.org/10.3390/w17010032
19. Sudha, D.; Dhanapandian, S.; Manoharan, C.; Arunachalam, A. Structural, morphological and electrical properties of pulsed electrodeposited $CdIn_2Se_4$ thin films. *Results Phys.* **2016**, *6*, 599–605. https://doi.org/10.1016/j.rinp.2016.09.004
20. Rawat, S.; Singh, J. Synthesis of nZnO from waste batteries by hydrometallurgical method for photocatalytic degradation of organic pollutants under visible light irradiation. *J. Environ. Manage.* **2022**, *318*, 115518. https://doi.org/10.1016/j.jenvman.2022.115518
21. Riwayati, I.; Winardi, S.; Madhania, S.; Shimada, M.; Kusdianto. Green synthesis of ZnO nanoparticles using Cosmos caudatus: Effects of calcination temperature and precursor type on photocatalytic and antimicrobial activities. *Res. Eng.* **2024**, *24*, 103594. https://doi.org/10.1016/j.rineng.2024.103594
22. Pholnak, C.; Sirisathitkul, C.; Suwanboon, S.; Harding, D.J. Effects of Precursor Concentration and Reaction Time on Sonochemically Synthesized ZnO Nanoparticles. *Mater. Res.* **2014**, *17*¸ 405-411. https://doi.org/10.1590/S1516-14392013005000192
23. Abdullah, J.A.A.; Guerrero, A.; Romero, A. Efficient and Sustainable Synthesis of Zinc Salt-Dependent Polycrystal Zinc Oxide Nanoparticles: Comprehensive Assessment of Physicochemical and Functional Properties. *Appl. Sci.* **2024**, *14*, 1815. https://doi.org/10.3390/app14051815
24. Nandiyanto, A.B.D.; Ragadhita, R.; Fiandini, M. Interpretation of Fourier Transform Infrared Spectra (FTIR): A Practical Approach in the Polymer/Plastic Thermal Decomposition. *IJoST* **2023**, *8*, 113-126. https://doi.org/10.17509/ijost.v8i1.53297
25. de Peres, M.L.; de Avila Delucis, R.; Amico S.C.; Gatto, D.A. Zinc oxide nanoparticles from microwave-assisted solvothermal process: Photocatalytic performance and use for wood protection against xylophagous fungus. *NMNT* **2019**, *9*, 1-8. https://doi.org/10.1177/1847980419876201
26. Zhu, F.; Persson, D.; Thierry, D.; Taxen, C. Formation of Corrosion Products on Open and Confined Zinc Surfaces Exposed to Periodic Wet/Dry Conditions. *Corrosion* **2000**, *56*, 1256-1265. DOI:10.5006/1.3280514